3D Local Measurements of Bone Strain and Displacement: Comparison of Three Digital Volume Correlation Approaches

Marco Palanca
School of Engineering and Architecture, University of Bologna
Via Terracini 28, Bologna, 40131, IT
marco.palanca2@unibo.it

Gianluca Tozzi
School of Engineering, University of Portsmouth
Anglesea Building, Anglesea Road, Portsmouth, PO1 3DJ, UK
gianluca.tozzi@port.ac.uk

Luca Cristofolini
School of Engineering and Architecture, University of Bologna
Viale Risorgimento 2, Bologna, 40136, IT
luca.cristofolini@unibo.it

Marco Viceconti
Department of Mechanical Engineering and INSIGNEO Institute for In Silico Medicine, University of Sheffield
Sir Frederick Mappin Building, Pam Liversidge building, Sheffield, S1 3JD, UK
m.viceconti@sheffield.ac.uk

Enrico Dall'Ara*
Department of Mechanical Engineering and INSIGNEO Institute for In Silico Medicine, University of Sheffield
Sir Frederick Mappin Building, Pam Liversidge building, Sheffield, S1 3JD, UK
e.dallara@sheffield.ac.uk

ABSTRACT (SHORT)

This study aimed to compare accuracy and precision errors of three Digital Volume Correlation (DVC) approaches in a particular 3D zero-strain condition for both trabecular and cortical bone specimens, imaged repeatedly using micro-CT. Both scalar average errors and errors affecting the individual components of displacements and strains were calculated. For each DVC approach, errors decreased asymptotically for larger sub-volume sizes in the range explored. Considering this particular set of images, the global approach (ShIRT-FE) showed an overall better accuracy and precision than the local ones (DaVis). The latter show reasonable results for large nodal spacing, particularly for trabecular bone.

ABSTRACT (LONG)

Background. Different Digital Volume Correlation (DVC) approaches are currently available or under development for bone tissue micromechanics. The aim of this study was to compare accuracy and precision errors of three DVC approaches for a particular 3D zero-strain condition.
Method of approach. Trabecular and cortical bone specimens were repeatedly scanned with a micro-CT. The errors affecting computed displacements and strains were extracted for a known virtual translation, as well as for repeated scans. Three DVC strategies were tested: two local approaches, based on Fast-Fourier-transform (DaVis-FFT) or Direct-Correlation (DaVis-DC), and a global approach based on elastic registration and a finite element solver (ShIRT-FE). Different computation sub-volume sizes were tested.
Results. Much larger errors were found for the repeated scans, than for the virtual translation test. For each algorithm, errors decreased asymptotically for larger sub-volume sizes in the range explored. Considering this particular set of images, ShIRT-FE showed an overall better accuracy and precision (a few hundreds microstrain for a sub-volume of 50 voxels). When the largest sub-volume (50-52 voxels) was applied to cortical bone, the accuracy error obtained for repeated scans with ShIRT-FE was approximately half of that for the best local approach (DaVis-DC). The difference was lower (250 microstrain) in the case of trabecular bone. In terms of precision, the errors shown by DaVis-DC were closer to the ones computed by ShIRT-FE (differences of 131 microstrain and 157 microstrain for cortical and trabecular bone, respectively). The multi-pass computation available for DaVis software improved the accuracy and precision only for the DaVis-FFT in the virtual translation, particularly for trabecular bone. The better accuracy and precision of ShIRT-FE, followed by DaVis-DC, were obtained with a higher computational cost when compared to DaVis-FFT.
Conclusions. The results underline the importance of performing a quantitative comparison of DVC methods on the same set of samples by using also repeated scans, other than virtual translation tests only. ShIRT-FE provides the most accurate and precise results for this set of images. However, both DaVis approaches show reasonable results for large nodal spacing, particularly for trabecular bone. Finally, this study highlights the importance of using sufficiently large sub-volumes, in order to achieve better accuracy and precision.

Keywords. Digital volume correlation, registration, micro-CT, zero-strain test, bone, accuracy, precision.

INTRODUCTION

Digital Volume Correlation (DVC) is a novel and useful tool for quantifying the internal 3D deformation across the entire volume of various biological tissues, such as bone [1]. In fact, DVC was originally developed by Bay and co-workers [2] to investigate the volumetric strain distribution throughout the bone trabecular structure. This was done to overcome the limitation of its 2D counterpart, known as digital image correlation (DIC), which has the ability to compute strain and displacement fields only on the external surface of the specimen [3]. The benefit of DVC relies in the use of volumetric images, that can be obtained by methods such as magnetic resonance imaging (MRI) [4], microscopy [5], computed tomography (CT), or high-resolution micro-CT [6-10], to track the deformation of internal features, by registering elastically the images of undeformed and deformed specimens. The procedure outputs a full-field 3D displacement vector. Afterwards, the displacement fields are differentiated using various numerical differentiation approaches to obtain full-field strain maps [11].

Since it was introduced, DVC in combination with micro-CT allowed the determination of displacement and strain field inside trabecular bone [2, 6, 8, 9], cortical bone [9, 12], trabecular bone substitutes [7], Aluminum foams [13] and also trabecular/cortical-cement composites [10]. However, DVC employs a number of computational strategies to recognize the features of the undeformed (fixed) and deformed (moved) volumes and, therefore, to provide estimates of displacement and strain distribution. Comparison studies among different DVC approaches are mandatory as accuracy and precision may vary significantly, depending on factors such as quality of the images,

typology of the specimen under investigation and intrinsic nature of the computational approach [1, 9, 10]. In fact, while numerical and experimental methods can validate each other if similar testing arrangements are defined, there is no golden standard to date for the assessment of the accuracy and precision of a DVC strategy, due to the unavailability of other accurate techniques able to measure internal strains. A first attempt to compare different DVC approaches used to investigate the performance of a trabecular bone substitute (porous polymeric scaffold) was carried out by Madi et al. [7], who compared the output of a local correlation algorithm based on Fast Fourier Transform (FFT) and another one based on a continuous and global home-written code [14, 15]. However, in Madi et al. [7] displacement and strain uncertainties of the two DVC methodologies were assessed only in relation to a virtual imposed rigid displacement test. Hence, the strain fluctuation associated with repeated scans [6, 9] was not considered.

The accuracy and precision of DVC in quantifying displacements and strains have been investigated for trabecular bone [6, 8, 9], cortical bone [9, 12] and whole bones [16, 17], where a single DVC software, either commercial or home-written, was employed. Moreover, in most cases errors are quantified in terms of average of the strain components [8, 9]. Only in one case the error affecting the DVC-computed single components of displacement and strain has been quantified for trabecular bone [6]. For all these reasons, further comparative accuracy investigations of DVC methodologies are needed to interpret the results obtained in bone applications. Only in this way the suitability of a specific DVC approach can be evaluated against both bone structure (i.e.

cortical, trabecular, cortical and trabecular together) and 'scale' of examination (i.e. dimension of the specimen, particular set of loading conditions).

The aim of this study was to perform a more extensive validation of the DVC, to better elucidate the sources of error affecting both displacement and strain calculations at the tissue level. Specifically, we compared the output of three different DVC approaches applied on the same micro-CT scanned specimen (trabecular and cortical bone) by investigating:

- The accuracy and precision in computing the displacement and strain fields for two zero-strain conditions: a virtually simulated 3D rigid displacement, and a specimen re-scan condition;
- The influence of different computation settings on the final outputs;
- The presence of preferential directions for strain measurement in the different algorithms.

MATERIAL AND METHODS

Specimens and images

Two specimens (Fig. 1) were obtained from a fresh bovine femur: a cylinder of cortical bone was extracted from the diaphysis (3 mm diameter, 20 mm height), and a cylinder of trabecular bone was extracted from the greater trochanter (8 mm diameter, 12 mm height). The specimens were already used in a previous study [9] and were collected from an animal sacrificed for alimentary purposes.

In order to compare the displacement and strain uncertainties using different DVC techniques, virtual image translation and zero-strain repeated scans [8] were employed. Micro-CT scans were performed in saline solution (SkyScan 1172, Bruker, Belgium; scanned height: 9.323 mm; 10 Megapixels 12-bit digital cooled ORCA-HR CCD; 2000 x 1048 pixel; 1 mm Aluminum beam hardening filter; power: 10 W; voltage: 59 kV for the trabecular bone and 70 kV for the cortical bone; voxel size: 9.96 micrometer; exposure: 1180 ms; rotation step: 0.7°; total rotation 180°; images averages: x2). Each specimen was scanned twice [9], without any repositioning between the scans (Scan1 and Scan2). In order to avoid possible artifacts due to small movements of free trabeculae at the outer surface, a volume of interest (VOI) consisting of a parallelepiped with a section of 180 voxels x 180 voxels and a height of 932 voxels, was cropped in the central portion of the scanned cylinders. Two tests were performed on the VOI extracted from both cortical and trabecular specimens (Fig. 1):

- "Repeated-Scan-Test": Scan1 and Scan2 were correlated in order to obtain a condition of zero-strain and real displacements, due to the machine micro-movements.
- "Virtually-Moved-Test": Scan1 was virtually translated of two voxels (19.92 micrometer) in each direction (Scan1_Moved) in order to obtain a known, controlled displacement with a zero-strain field. Correlation of Scan1_Moved was computed with reference to the original Scan1. A bounding box of ten voxels was added all around the specimen in order to avoid losing part of the image.

The cropping and translation were performed by means of a free imaging processing toolkit MeVisLab (MeVis Medical Solution AG, http://www.mevislab.de/).

DVC approaches under investigation

The outputs of three DVC approaches were compared (Fig. 2), for both specimens and for both Repeated-Scan-Test and Virtually-Moved-Test.

The first two approaches are implemented in a commercial DVC software: DaVis 8.2.1 (LaVision Ltd, Goettingen, Germany). The volume correlation begins with the division of the 3D images into smaller and selectable sub-volumes, represented as a discrete function of grey levels. Recognition of identical features is possible via Fast-Fourier-transform (FFT, later referred to as "Davis-FFT") [6, 7] or via Direct-Correlation (DC, later referred to as "Davis-DC") [18]. Either way, a piece-wise linear shape function for the reference-deformed mapping and a cross-correlation function are employed to quantify the similarity between the images [6, 7]. For both DaVis-FFT and DaVis-DC, a normalized cross-correlation coefficient, r_{DaVis}, based on grey level gaps is used:

$$r_{DaVis} = \frac{\sum_{\underline{X}(x,y,z)\in VOI} f(x,y,z)g(x',y',z')}{\sqrt{\sum_{\underline{X}(x,y,z)\in VOI} f(x,y,z)^2 \sum_{\underline{X}^*(x,y,z)\in VOI} g(x',y',z')^2}} \qquad \text{(Eq. 1)}$$

where: X (x, y, z) and X*(x, y, z) refer to coordinates (in voxels) of a same point in the initial state and in the deformed state; f and g are the grey levels respectively in the initial and deformed images. The main difference between DaVis-FFT and DaVis-DC lies on the use of a Fourier space for the calculation in DaVis-FFT [19], rather than a direct

coupling for DaVis-DC. A tri-linear interpolation is used in the case of DaVis-FFT, and a 3rd order spline interpolation in DaVis-DC. The estimated full 3D displacement field is then computed, with sub-voxel precision, through a predictor-corrector approach with decreasing subset sizes, and an intensity interpolation Gaussian algorithm fitted to the correlation peak. This process, also known as multi-pass, allows the calculated displacements from the predictor step to be used to inform the next corrector step. The process is iterated as the sub-volume size decreases to its final defined size. This process provides a full 3D field of displacement vectors, which describes the mapping from reference to deformed state. From the field of resultant displacement vectors at the center of each sub-volume, the field of strain components is computed using a centered finite difference scheme.

The third approach (later referred to as "ShIRT-FE") consists in combining a home-written elastic registration software ShIRT [4, 5, 20] with a Finite Element (FE) simulation in ANSYS Mechanical APDL v.14.0 (Ansys Inc., USA). The procedure, reported in [9], focuses on the recognition of identical features in the two 3D images by superimposing a homogeneous cubic grid with certain nodal spacing (sub-volume) to the images to be registered. The software computes the nodal displacements that map each point in the first image (Scan1), into the ones in the second image (Scan2), solving the equations in the nodes of the grid [9, 20]. Briefly, the procedure consists in finding the displacement functions $u(x,y,z)$, $v(x,y,z)$ and $w(x,y,z)$ that map the fixed image $\boldsymbol{f}(x,y,z)$ into the moving image $\boldsymbol{m}(x',y',z')$. As described in Barber et al. [4] an additional

intensity displacement function *c(x, y, z)* is included in order to account for changes in the grey levels. For small displacement values we need to solve:

$$\boldsymbol{f}-\boldsymbol{m} \approx \frac{1}{2}\left(u\left(\frac{\partial \boldsymbol{f}}{\partial x}+\frac{\partial \boldsymbol{m}}{\partial x}\right)+v\left(\frac{\partial \boldsymbol{f}}{\partial y}+\frac{\partial \boldsymbol{m}}{\partial y}\right)+w\left(\frac{\partial \boldsymbol{f}}{\partial z}+\frac{\partial \boldsymbol{m}}{\partial z}\right)-c(\boldsymbol{f}+\boldsymbol{m})\right) \qquad \text{(Eq. 2)}$$

However, as this problem would be underdetermined if solved for each voxel, ShIRT solves the equations only in the nodes of a cubic grid superimposed to the images and with elements as large as the imposed sub-volume. The displacements are interpolated with a tri-linear function between the nodes. The problem is then solved when the coefficients $\boldsymbol{a}$ of the displacement functions are found:

$$\begin{cases} u = \sum_i a_{xi}\varphi_i \\ v = \sum_i a_{yi}\varphi_i \\ w = \sum_i a_{zi}\varphi_i \end{cases} \qquad \text{(Eq. 3)}$$

ShIRT adds an additional smoothness constraint on the mapping by including in the solution a term based on the Laplacian operator $\boldsymbol{L}$, and the coefficient λ that weights the relative importance of smoothing. Therefore, it can be demonstrated that for suitable values of λ, a robust solution is obtained by solving the following equation in matrix form:

$$(\boldsymbol{f}-\boldsymbol{m}) = (\boldsymbol{T}^{\boldsymbol{T}}\boldsymbol{T}+\boldsymbol{\lambda}\boldsymbol{L}^{\boldsymbol{T}}\boldsymbol{L})\boldsymbol{a} \qquad \text{(Eq. 4)}$$

where $\boldsymbol{T}$ is a KxN matrix (K number of voxels in the image, and N number of nodes in the grid). $\boldsymbol{T}$ is derived from integrals of the image gradients multiplied by the basis functions of the displacements. For large displacements the method can iterate to a correct solution as shown in [4]. The grid is then converted into an 8-noded hexahedrons mesh. The displacements computed by ShIRT at each node of the grid are

imposed as boundary conditions for the computation of the strain field with a commercial FE solver (ANSYS).

Influence of sub-volume size

In order to compare the results of the different DVC approaches an analysis on the dependency of the accuracy and precision in function of the selected sub-volume size (5-50 voxels) was performed (Table 1). In particular, for the DaVis approaches, no overlap or multi-pass approach was used for a fair comparison. However, a correlation using a multi-pass approach incorporated in DaVis for that specific VOI (extending the computation sub-volume up to 52 voxels, Table 2) was also implemented in order to investigate the effect of other features typical of the DaVis commercial software, for this specific type of images. As the DaVis software did not allow selecting any arbitrary sub-volume size when the DC was used for feature recognition, the nearest sub-volume size available was used (8-52 voxels).

Metrics to quantify the accuracy and precision

The components of displacement and strain were extracted from the different approaches and processed with a home-written script MatLab 2014a, (The MathWorks, Natick, USA). For the three approaches, accuracy (average) and precision (standard deviation-SD) were quantified for each component of the displacement. Quantitative comparisons were performed on the strains in two ways:

- Scalar comparison: in order to compare the outputs of the different approaches for strain estimation, following the indications available in literature [8, 9], accuracy and precision were quantified as the average and the SD of the average of the absolute values of the six strain components.
- Comparison by component: in order to investigate the presence of preferential components of strain in the algorithms, accuracy (average) and precision (SD) were reported and compared for each component of the strain.

The trends were analyzed plotting the errors as a function of the sub-volume sizes. Different interpolating laws were tested (linear, polynomial, power-law) in terms of adjusted determination coefficient.

Some sub-volumes could not be correlated by the DaVis algorithms (i.e. because they contained only voxels of constant intensity). Due to the algorithm locally normalizing the intensity, no correlation at all is possible for such sub-volumes, and as such, no corresponding displacement vector can be calculated. To avoid misinterpretation of the results, the correlated volume was evaluated for each computation sub-volume size (Table 1) as the ratio between the numbers of correlated voxels and the total number of voxels of the VOI. This applied to the DaVis approaches only, as of the ShIRT-FE the correlated volume is 100% by definition.

Finally, the computational cost of each approach was estimated as the sum of the computation time needed for the different analyses. For the DaVis-FFT and DaVis-DC the computation time was calculated as the total time for the feature recognition, the time necessary for the computation of the displacement field and the time needed

for the computation of the strain field. For the ShIRT-FE approach, the computational cost was estimated as the time needed for the registration with ShIRT plus the time for computing the strain with the FE solver.

RESULTS

The correlated volume (both trabecular and cortical bone) seemed to increase for the DaVis-FFT and to decrease for the DaVis-DC, as the computation sub-volume increased, although no clear trend was observed (Table 1). Because of the different computational approach, such analysis does not apply to the ShIRT-FE, which is based on a global analysis on the total volume.

Displacement

The comparison of the displacement among the different approaches is reported only for the "Virtually-Moved-Test", as the actual displacement in the "Repeated-Scan-Test" is unknown.

The accuracy errors for the displacements were comparable for the cortical and trabecular specimens (Table 3). For the different sub-volume sizes (from 5-8 to 50-52 voxels) and specimen types (trabecular and cortical), the largest accuracy error was found for the Davis-FFT approach (up to 13 micrometer), which was larger than those found with the Davis-DC (never exceeding 0.1 micrometer), and larger than those obtained with the ShIRT-FE (never exceeding 0.01 micrometer). The smallest accuracy

errors for the DaVis-FFT and DaVis-DC were found along the z-direction (i.e. the rotation axis of the micro-CT during imaging). Conversely, errors were slightly larger in the z-direction for ShIRT-FE. The tendency of the DaVis-FFT and ShIRT-FE was for an improved accuracy for larger sub-volume sizes.

Similarly, the largest precision errors (Table 4) were found for the DaVis-FFT (several micrometers), followed by DaVis-DC (between 0.1 and 1 micrometer), and then by the ShIRT-FE (never exceeding 0.1 micrometer). The smallest precision errors for the DaVis-FFT and DaVis-DC were found once more along the z-direction, whereas errors were slightly larger along the z-direction for ShIRT-FE. The precision of all three DVC approaches tended to improve as a function of the computation sub-volume size.

Strain

Scalar comparison

The first comparison is based on the scalar magnitudes, calculated similarly to [8].

For the "Virtually-Moved-Test", the errors for the strains were comparable for the cortical and trabecular specimens. Both the accuracy (Fig. 3) and the precision (Fig. 4) error were largest for the Davis-FFT (at best: 4670 and 1718 microstrain, respectively), which was larger than with Davis-DC (at best: 18 and 6 microstrain, respectively), and ShIRT-FE approach (below one microstrain). Both accuracy and precision showed a steady improvement for larger sub-volumes for all three DVC approaches, following a power-law relation (Fig. 3, 4). For the DaVis-FFT, the multi-pass

approach provided a better accuracy (Fig. 3) and precision (Fig. 4) than the same algorithm at 50 voxels. Conversely, the multi-pass approach did not improve the outcomes of the DaVis-DC at similar sub-volume size (52 voxels).

For the "Repeated-Scan-Test", the errors were larger for the cortical bone than for the trabecular bone. For all three DVC approaches, both accuracy (Fig. 5) and precision (Fig. 6) improved for larger sub-volumes, following a power-law relation. Similar trends to the "Virtually-Moved-Test" were observed, but with lower differences. The accuracy error for all approaches was between hundreds and thousands of microstrain for the best settings: errors were largest for the Davis-FFT, followed by the Davis-DC, and by the ShIRT-FE (Fig. 5). The lowest precision error was of the same order of magnitude for DaVis-DC and ShIRT-FE (a few hundreds of microstrain at best) and was larger for DaVis-FFT, particularly for the cortical bone (Fig. 6). In this test, the multi-pass approach provided worse accuracy and precision than the largest sub-volume alone, for both the DaVis-FFT and the DaVis-DC.

Comparison by components

When the individual components of strain were analyzed separately, the same trend was observed between the three computation approaches (worst: DaVis-FFT; best: ShIRT-FE), for both the accuracy and precision (Figs. 7-10).

In the "Virtually-Moved-Test" the accuracy (Fig. 7) and precision (Fig. 8) errors with the Davis-FFT and in particular Davis-DC were larger for the normal strain components, than for the shear strains. Among the normal strain components, errors

were smaller in the z-direction. Conversely, the accuracy error was similar for each component for the ShIRT-FE (and closer to zero than the DaVis-FFT and DaVis-DC).

No systematic difference was observed between strain components for the "Repeated-Scan-Test", although the accuracy (Fig. 9) and precision (Fig. 10) errors were generally larger for the normal strains.

Computational costs

The total computation times were:

- For the DaVis-FFT: 8 seconds for a computation sub-volume of 5 voxels, and 5 seconds for 50 voxels (3.4 GHz quad-core i7, 32 GB Ram, solid state disk);
- For the DaVis-DC: 146 seconds for a computation sub-volume of 8 voxels, and 80 seconds for 52 voxels (3.4 GHz quad-core i7, 32 GB Ram, solid state disk);
- For the ShIRT-FE: 404 seconds for a computation sub-volume of 5 voxels, and 120 seconds for 50 voxels (2.9 GHz dual-core i7, 8 GB Ram, solid state disk). This does not include the time for migrating from the correlation software to the FE package.

DISCUSSION

The aim of this study was to compare the accuracy and precision of different DVC approaches used in computing the displacements and strains from micro-CT images of cortical and trabecular bone. Three DVC approaches were tested in a zero-strain

condition (Repeated-Scan-Test) and with a virtual rigid displacement (Virtually-Moved-Test).

We investigated the strengths and limitations of two commercial approaches (DaVis-FFT and DaVis-DC) that implement different local correlation algorithms to estimate the displacement and strain fields, and a third approach (ShIRT-FE), which exploits a global correlation strategy, by combining an elastic registration algorithm to estimate the displacements, and an FE solver for computing the strain [9].

In this study, all the DVC approaches showed non-linear trends for the accuracy and precision of the strain, as a function of the considered sub-volume: the larger the sub-volume, the lower the error. However, it is important to remember that increasing the sub-volume size reduces the spatial resolution of the method. An inverse relationship between the size of the computation sub-volume and the displacement/strain uncertainties is typical for both local and global approaches [21]. Such trends were reported when DVC was applied to synthetic and natural trabecular bone [6, 7], and in a validation study on the DIC [22, 23]. The accuracy and precision of the three DVC approaches showed an asymptotic trend, when the sub-volume exceeded a size of 25-30 voxels for the displacements, and around 50 voxels for the strains. Given the voxel size (9.96 micrometers) this corresponds to the typical dimension of trabeculae (50-500 micrometers [24, 25]) and osteons (150-250 micrometers [24, 25]). This consideration could be the explanation for the slightly better behavior of the DVC applied to the trabecular bone (coarser pattern; closer to the ideal condition of 1:1 solid-porosity ratio) as opposed to the cortical one. It is possible to deduce that a

relatively large sub-volume investigated in this study (larger than 30 voxels) provides an optimal trade-off between spatial resolution, and error when applied to bone tissue. The three DVC approaches differed among each other in terms of accuracy and precision, both as a scalar (average of the error components, similarly to [8]), and for the individual components (similarly to [6]) of displacement and strain. The ShIRT-FE approach showed the best accuracy and precision for the displacements in the Virtually-Moved-Test. The errors on the displacements estimated by DaVis-DC were comparable with ShIRT-FE, while the errors affecting the DaVis-FFT were some order of magnitude higher. The accuracy and precision achieved on the displacements by ShIRT-FE and DaVis-DC with optimal settings (sub-volume larger than 25 voxels) were generally better than 0.1 micrometers. Such an accuracy and precision is sufficient for most applications with hard tissue. Consequently, as the strain field is obtained by differentiation of the displacement field in DaVis, similar trends were found for the errors affecting the computed strain. The best accuracy and precision achieved on the strains for the Repeated-Scan-Test by ShIRT-FE and DaVis-DC with optimal settings (sub-volume of 50-52 voxels) were of the order of a few hundred microstrain (in case of cortical bone up to 1053 and 477 microstrain for DaVis-DC and ShIRT-FE, respectively). Such an error is one order of magnitude lower than the failure strain of bone tissue (7000 microstrain in tension, 10000 microstrain in compression, [26]). Therefore, one can at least discriminate between yielded and not-yielded regions. However, the present results suggest that, in order to further improve the accuracy and precision, larger computation sub-volumes should be used, with the concurrent limitations in terms of resolution.

While for the cortical bone the differences among the approaches were higher, in case of trabecular bone the DaVis-DC approach provided accuracy and in particular precision closer to the ShIRT-FE approach, when moving towards larger sub-volumes. When making such comparisons one should remember that the global approach (ShIRT-FE) is based on a method where each element is affected by up to eight neighboring elements [7]. In fact, the improvement of accuracy and precision we found may be, among the other parameters, driven by the continuity assumption. The results of this study for the repeated scans confirm that similar uncertainty levels are obtained for a global approach (ShIRT-FE) with a mesh two times finer than the one used for a local one (DaVis-FFT) [21]. Moreover, it should be also noted that the precision and accuracy errors for the DaVis-DC were underestimated as the solution covered a lower correlated volume (80% for sub-volume equal to 52 voxels): if the entire VOI was forcedly included (including regions affected by poor correlation), the overall error would have been larger. Further studies in this direction will be done in the future in order to quantify these effects.

To the Authors' knowledge, this is the first paper that compares three different DVC approaches, and different bone microstructures. In reference [7] two DVC approaches were compared, on a single porous polymeric specimen and only for a virtual rigid displacement. Similarly to our study, they concluded that a global correlation approach gives lower errors than a local DVC algorithm. However, it was also reported how, for that particular specimen and set of images, the local FFT-based approach (DaVis-FFT) might be appropriate and provided a good compromise between

computational cost and accuracy (strain uncertainties of the order of 200 microstrain from virtually moved test). Conversely, in our study the DaVis-FFT approach showed high accuracy and precision errors for the cortical bone and, therefore, should be used carefully with similar images.

In order to understand the true reliability of the strain and displacement results one should also consider the correlated volume, or the quantity of numerical outputs (i.e. displacements) relative to either the software calculation scheme, or a specific threshold chosen for the correlation function. Hence, using local algorithms (DaVis-FFT and DaVis-DC) there may be cases where a very small error can be achieved at the cost of excluding large regions that would increase the error indicators. In this study, no specific threshold value for the correlation function was adopted in DaVis. However, a certain amount of data is systematically lost in the correlation of sub-volumes containing voxels with constant intensities, due to the algorithm local normalization.

The selected sequence of sub-volumes (96-64-52), overlaps (50%-50%-75%) and iterations (1-2-3), used in this study for the multi-pass calculation in DaVis approaches (Table 2), did only improve the performance of DaVis-FFT for the Virtually-Moved-Test, in particular for the trabecular bone. This can be used as a valuable indication for future studies, where the same multi-pass cannot be used as a universally valid matrix for all the cases and approaches, but parameters may be selected for that specific bone tissue, test, quality of images and sample size.

In terms of computational cost, the DaVis-FFT and DaVis-DC were lighter than ShIRT-FE. Between the two local algorithms, DaVis-DC was up to two orders of

magnitude slower. It must be noted that while DaVis-FFT has been implemented earlier and was fully optimized in terms of computational efficiency, the current versions of DaVis-DC and of ShIRT-FE were not yet fully optimized. For further application on larger VOIs, and considering that the DVC is becoming increasingly common, a reduced computation time would be desirable.

In this study a step beyond the work of [8] and [9] was done in order to investigate if strain components are better evaluated in some preferential direction. In fact, for both the Virtually-Moved-Test and the Repeated-Scan-Test, ShIRT-FE showed a more isotropic behavior, with similar errors for the six components of the strain. Conversely, in the Virtually-Moved-Test the DaVis-FFT and in particular DaVis-DC approaches showed better accuracy (Fig. 7) and precision (Fig. 8) for the shear strains than for the normal strain components, consistently with the findings reported by [6]. For these approaches it must be noted that when a scalar indicator of the error is computed averaging the different strain components (similarly to [8] and [9], Fig. 3-6), this underestimates by about 50% the largest error, which is found for just one of the strain components (Fig. 7-10, DaVis-FFT and DaVis-Dc). However, these trends became less clear in the more interesting case of the Repeated-Scan-Test where, for all three approaches, similar errors were found for all strain components and highest errors were generally produced for one of the normal strains. In such a case, reporting the error in terms of averages is less critical.

A limitation of this work relates to the number of specimens: only one for the cortical bone and one for trabecular bone. Moreover, due to the limited diameter of

the cortical bone specimen, only a limited range of sub-volume sizes was explored. The dimensions of the specimens were suitable for bone tissue, considering its osteomorphometric parameters [27]. Potential influences of specimen size (i.e. whole vertebra), image quality (i.e. variation of the level of noise) and scanning resolution (i.e. clinical CT) on the accuracy and precision obtainable with different DVC approaches (i.e. optimal multi-pass calculation for DaVis-FFT and DaVis-DC), are yet to be investigated. Moreover, in this study only trabecular and cortical specimens were considered. Further analysis shall be conducted on specimens composed of both cortical and trabecular tissue, and possibly incorporating biomaterials (i.e. implantable devices or injectable materials).

CONCLUSION

In conclusion, we have shown the importance of performing a quantitative optimization and validation of DVC approaches by using repeated scans and comparing the DVC outputs on the same set of specimens. While computed displacements were generally highly accurate and precise, larger errors (decreasing with larger sub-volumes and with a similar behavior for each component) were found in the computed strain distributions. Our results show how the integration of DVC (for the computation of displacements) with an FE code (which imposes a continuum mechanics assumption on the structure) provides the most accurate and precise results, for this particular set of images. However, the local DaVis approaches, as a single software package, show reasonable results for large nodal spacing and particularly for trabecular bone. The results from the repeated scans showed that the multi-pass calculation scheme used in

this study for the DaVis methods lead to larger errors compared to the largest sub-volume. Moreover, the errors from the Repeated-Scan-Test were similar for the different components for all three methods. Finally, this study indicates that every method should be used with sufficiently large sub-volumes in order to achieve reasonable accuracy and precision. Further work is needed to fully appreciate the performance of DVC for different bone structures, dimensions and imaging techniques/settings.

ACKNOWLEDGMENTS

The Authors gratefully acknowledge the technical support ad advice of Dr Dave Hollis (LaVision Ltd, UK) and Prof David Barber for sharing the ShIRT registration script.

FUNDING

This study was partially funded by the FP7 European program (MAMBO: PIEF-GA-2012-327357) and Royal Society Research Grant (RG130831).

NOMENCLATURE

DVC	Digital volume correlation
ShIRT	Sheffield image registration toolkit
DIC	Digital image correlation
FFT	Fast Fourier transform
VOI	Volume of interest
FE	Finite element
SD	Standard deviation
R^2	Coefficient of determination
CT	Computed tomography
CFD	Centered finite difference

FIGURE CAPTIONS

Figure 1 – Schematic of the two specimens obtained from a fresh bovine femur: a cylinder of cortical bone was extracted from the diaphysis (3 mm diameter, 20 mm height), and a cylinder of trabecular bone was extracted from the greater trochanter (8 mm diameter, 12 mm height). Each specimen was scanned twice (height of 9.323 mm). Identical Volumes of Interest (VOI) were extracted from each specimen. The displacements and strains were computed for such a zero-strain condition, both between Scan 1 and Scan 2, and by virtually displacing Scan 1.

Figure 2 – Description of the three DVC approaches for the determination of strain accuracy and precision. DaVis software enabled both Fast Fourier Transform (DaVis-FFT) and Direct Correlation (Davis-DC) displacement calculation and strain was computed using a Centered Finite Difference (CFD) scheme. A custom-written software (ShIRT) in combination with a finite element (FE) solver was also tested.

Figure 3 – Virtually-Moved-Test: trend of the accuracy (microstrain) for both cortical and trabecular specimen, as a function of the sub-volume size (voxels). The accuracy of the three DVC approaches was first computed as a scalar, consistently with Liu & Morgan, 2007). The trendline equation (power-law relation and R^2) is also reported.

*The sub-volume was different for DaVis-DC. Refer to Table 1 for more details.

Figure 4 – Virtually-Moved-Test: trend of the precision (microstrain) for both cortical and trabecular specimen, as a function of the sub-volume size (voxels). The precision of

the three DVC approaches was first computed as a scalar, consistently with Liu & Morgan, 2007). The trendline equation (power-law relation and R^2) is also reported.

* The sub-volume was different for DaVis-DC. Refer to Table 1 for more details.

Figure 5 – Repeated-Scan-Test: trend of the accuracy (microstrain) for both cortical and trabecular specimen, as a function of the sub-volume size (voxels). The accuracy of the three DVC approaches was first computed as a scalar, consistently with Liu & Morgan, 2007). The trendline equation (power-law relation and R^2) is also reported.

* The sub-volume was different for DaVis-DC. Refer to Table 1 for more details.

Figure 6 – Repeated-Scan-Test: trend of the precision (microstrain) for both cortical and trabecular specimen, as a function of the sub-volume size (voxels). The precision of the three DVC approaches was first computed as a scalar, consistently with Liu & Morgan, 2007). The trendline equation (power-law relation and R^2) is also reported.

* The sub-volume was different for DaVis-DC. Refer to Table 1 for more details.

Figure 7 – Virtually-Moved-Test: Analysis of the accuracy of the six components of strain (microstrain), in both cortical and trabecular specimen, for the largest sub-volume size considered (50 voxels ShIRT & DaVis-FFT, 52 voxels DaVis-DC). The Z-axis represents the axis of rotation of the specimen during imaging in the micro-CT. The accuracy of the three DVC approaches was computed as the average of the absolute values of each component of strain. Different scales are used for the three computation approaches due to large differences in absolute values.

Figure 8 – Virtually-Moved-Test: Analysis of the precision of the six components of strain (microstrain), in both cortical and trabecular specimen, for the largest sub-volume size considered (50 voxels ShIRT & DaVis-FFT, 52 voxels DaVis-DC). The Z-axis represents the axis of rotation of the specimen during imaging in the micro-CT. The precision of the three DVC approaches was computed as the standard deviation of the absolute values of each component of strain. Different scales are used for the three computation approaches due to large differences in absolute values.

Figure 9 – Repeated-Scan-Test: Analysis of the accuracy of the six components of strain (microstrain), in both cortical and trabecular specimen, for the largest sub-volume size considered (50 voxels ShIRT & DaVis-FFT, 52 voxels DaVis-DC). The Z-axis represents the axis of rotation of the specimen during imaging in the micro-CT. The accuracy of the three DVC approaches was computed as the average of the absolute values of each component of strain. Different scales are used for the three computation approaches due to large differences in absolute values.

Figure 10 – Repeated-Scan-Test: Analysis of the precision of the six components of strain (microstrain), in both cortical and trabecular specimen, for the largest sub-volume size considered (50 voxels ShIRT & DaVis-FFT, 52 voxels DaVis-DC). The Z-axis represents the axis of rotation of the specimen during imaging in the micro-CT. The precision of the three DVC approaches was computed as the standard deviation of the absolute values of each component of strain. Different scales are used for the three computation approaches due to large differences in absolute values.

Table Caption List

Table 1 Comparison of the correlated volumes for the different computation approaches, for both specimens (cortical and trabecular) and both tests, and according to the size of the sub-volume.

***Note**: In the ShIRT-FE approach the computation occurs only in the nodes of the elements of the selected grid. Although the number of measurement points was less than the number of measurement points of the other two approaches (DaVis-FFT and DaVis-DC), this allows a correlation on the whole volume.

Table 2 Parameters used in the multi-pass approach for both the DaVis-FFT and the DaVis-DC.

Table 3 Accuracy of the computed components of displacement (micrometer) in the Virtually-Translated-Test for the three DVC approaches and different sub-volumes in both cortical and trabecular specimen. The z-direction is the axis of rotation of the specimen during imaging in the micro-CT.

Table 4 Precision of the computed components of displacement (micrometer) in the Virtually-Translated-Test for the three DVC approaches and different sub-volumes in both cortical and trabecular specimen. The z-direction is the axis of rotation of the specimen during imaging in the micro-CT.

Table 1

		DaVis-FFT		DaVis-DC		ShIRT-FE	
	Nominal sub-volume size (voxels)	Actual sub-volume size (voxels)	Correlated volume (%)	Actual sub-volume size (voxels)	Correlated volume (%)	Actual sub-volume size (voxels)	Correlated volume (%)
Cortical Virtually-Moved-Test	5	5	25.9%	8	100.0%	5	100%*
	10	10	79.5%	10	100.0%	10	
	15	15	100.0%	16	100.0%	15	
	20	20	100.0%	20	99.2%	20	
	25	25	100.0%	24	99.3%	25	
	30	30	97.2%	28	99.6%	30	
	35	35	100.0%	34	96.6%	35	
	40	40	100.0%	40	96.7%	40	
	45	45	100.0%	44	84.4%	45	
	50	50	100.0%	52	96.6%	50	
Trabecular Virtually-Moved-Test	5	5	30.3%	8	100.0%	5	100%*
	10	10	79.8%	10	100.0%	10	
	15	15	100.0%	16	100.0%	15	
	20	20	100.0%	20	99.2%	20	
	25	25	100.0%	24	99.3%	25	
	30	30	97.2%	28	99.6%	30	
	35	35	99.9%	34	96.6%	35	
	40	40	100.0%	40	96.7%	40	
	45	45	100.0%	44	84.4%	45	
	50	50	100.0%	52	96.6%	50	
Cortical Repeated-Scan-Test	5	5	37.1%	8	100.0%	5	100%*
	10	10	94.4%	10	100.0%	10	
	15	15	100.0%	16	99.9%	15	
	20	20	100.0%	20	99.1%	20	
	25	25	100.0%	24	99.3%	25	
	30	30	100.0%	28	99.9%	30	
	35	35	100.0%	34	99.9%	35	
	40	40	100.0%	40	99.7%	40	
	45	45	100.0%	44	98.5%	45	
	50	50	91.8%	52	79.6%	50	
Trabecular Repeated-Scan-Test	5	5	45.4%	8	100.0%	5	100%*
	10	10	95.8%	10	100.0%	10	
	15	15	100.0%	16	99.9%	15	
	20	20	99.9%	20	99.1%	20	
	25	25	100.0%	24	99.3%	25	
	30	30	100.0%	28	99.9%	30	
	35	35	100.0%	34	99.9%	35	
	40	40	100.0%	40	99.7%	40	
	45	45	100.0%	44	98.5%	45	
	50	50	91.8%	52	79.6%	50	

Table 2

Step	Sub-volume size (voxels)	Overlap between sub-volumes	Number of iterations
1	96	50%	1
2	64	50%	2
3	52	75%	3

Table 3

		DaVis-FFT			DaVis-DC			ShIRT-FE		
	Nominal Sub-volume size (voxels)	Accuracy along x-axis (micrometers)	Accuracy along y-axis (micrometers)	Accuracy along z-axis (micrometers)	Accuracy along x-axis (micrometers)	Accuracy along y-axis (micrometers)	Accuracy along z-axis (micrometers)	Accuracy along x-axis (micrometers)	Accuracy along y-axis (micrometers)	Accuracy along z-axis (micrometers)
CORTICAL BONE	**5**	13.54	13.18	14.11	0.0019	0.0019	0.00045	0.0015	0.0013	0.00073
	10	5.02	4.43	5.98	0.0079	0.0079	0.0017	0.00044	0.00023	0.00041
	15	5.10	4.78	4.47	0.080	0.079	0.013	0.00047	0.00101	0.0029
	20	5.02	4.74	3.94	0.026	0.033	0.054	0.0000059	0.000081	0.0000080
	25	5.00	4.76	3.59	0.04	0.04	0.0017	0.0000091	0.0000068	0.0000044
	30	4.18	3.95	3.13	0.047	0.047	0.0084	0.00018	0.00016	0.000501
	35	4.32	4.12	3.16	0.052	0.052	0.0099	0.00027	0.000014	0.000025
	40	5.25	5.07	2.90	0.063	0.064	0.008	0.0027	0.000053	0.00015
	45	3.66	3.39	2.88	0.052	0.051	0.00033	0.000022	0.0000050	0.000018
	50	5.47	5.26	2.96	0.074	0.074	0.0095	0.0000032	0.0000047	0.000012
TRABECULAR BONE	**5**	14.48	14.33	14.86	0.0011	0.0013	0.00074	0.0012	0.0012	0.0013
	10	7.79	7.50	9.27	0.0034	0.0056	0.00062	0.00034	0.00025	0.00089
	15	8.75	8.55	9.23	0.0092	0.011	0.0012	0.00068	0.00071	0.0029
	20	9.21	8.97	9.58	0.014	0.00065	0.018	0.000080	0.000042	0.000034
	25	9.43	9.33	9.51	0.0083	0.011	0.0031	0.000011	0.000016	0.000022
	30	9.42	9.28	9.12	0.0097	0.011	0.0014	0.0000088	0.000096	0.000047
	35	9.35	9.10	8.84	0.012	0.011	0.0029	0.000048	0.0000023	0.000011
	40	8.67	8.31	8.37	0.012	0.011	0.00099	0.000403	0.000028	0.00016
	45	8.54	8.22	7.61	0.012	0.012	0.0012	0.000045	0.000004	0.000012
	50	7.14	6.96	6.85	0.012	0.011	0.0011	0.0000026	0.0000004	0.0000098

Table 4

		DaVis-FFT			DaVis-DC			ShIRT-FE		
	Nominal Sub-volume size (voxels)	Precision along x-axis (micrometers)	Precision along y-axis (micrometers)	Precision along z-axis (micrometers)	Precision along x-axis (micrometers)	Precision along y-axis (micrometers)	Precision along z-axis (micrometers)	Precision along x-axis (micrometers)	Precision along y-axis (micrometers)	Precision along z-axis (micrometers)
CORTICAL BONE	**5**	6.62	6.73	6.53	0.32	0.33	0.17	0.086	0.086	0.37
	10	8.12	8.04	7.40	0.15	0.16	0.093	0.017	0.017	0.067
	15	5.29	5.20	5.36	0.22	0.22	0.093	0.019	0.019	0.077
	20	4.87	4.84	3.92	1.06	1.03	0.42	0.0024	0.0023	0.0092
	25	4.83	4.81	3.44	0.078	0.079	0.054	0.00093	0.00095	0.00044
	30	3.93	3.89	2.75	0.082	0.081	0.04	0.0037	0.0037	0.014
	35	3.85	3.81	2.95	0.085	0.085	0.041	0.00093	0.00066	0.00074
	40	4.37	4.32	2.48	0.087	0.086	0.038	0.0057	0.0011	0.0036
	45	3.67	3.52	2.76	0.082	0.081	0.054	0.00063	0.00054	0.00076
	50	3.94	3.88	2.88	0.084	0.084	0.039	0.00013	0.00013	0.00016
TRABECULAR BONE	**5**	6.19	6.22	5.79	0.35	0.33	0.28	0.087	0.087	0.37
	10	8.37	8.24	7.30	0.19	0.18	0.21	0.017	0.017	0.068
	15	7.38	7.05	7.05	0.11	0.11	0.15	0.019	0.019	0.078
	20	7.29	6.98	6.79	0.66	0.57	0.22	0.0025	0.0025	0.0097
	25	7.22	6.78	6.95	0.07	0.059	0.089	0.00093	0.00095	0.00045
	30	6.90	6.49	6.82	0.054	0.045	0.064	0.0033	0.0033	0.012
	35	6.63	6.14	6.57	0.036	0.032	0.039	0.00058	0.00065	0.00075
	40	6.36	5.87	6.32	0.026	0.023	0.028	0.0014	0.00105	0.0034
	45	5.55	5.12	5.73	0.024	0.021	0.018	0.00059	0.00052	0.00073
	50	5.10	4.72	5.17	0.016	0.016	0.015	0.00011	0.00011	0.00014

Figure1

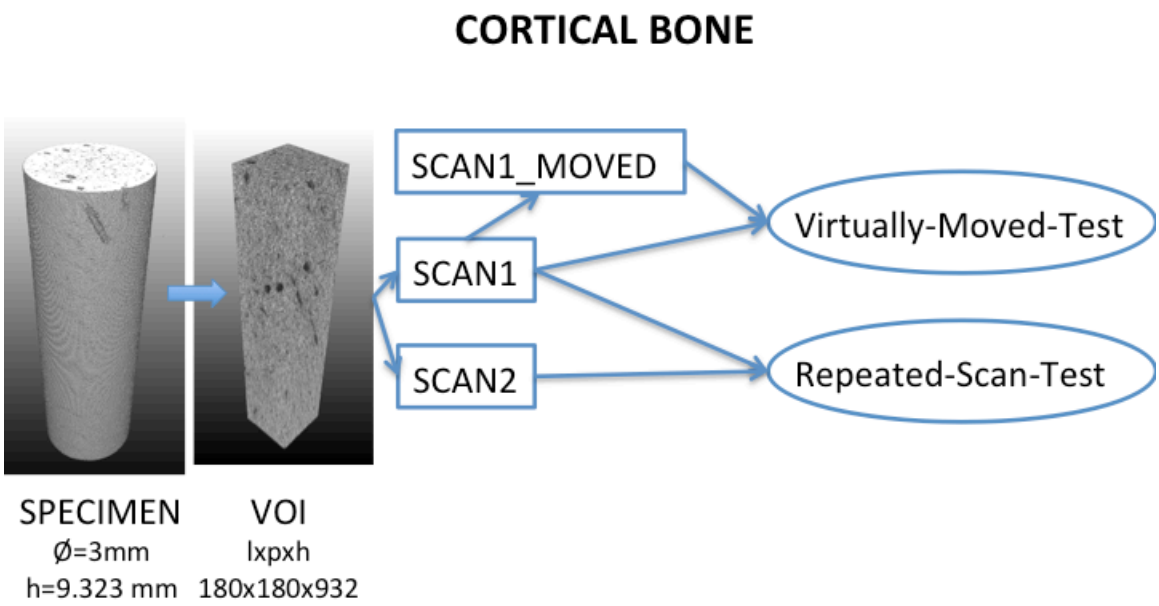
CORTICAL BONE
SCAN1_MOVED
SCAN1
SCAN2
Virtually-Moved-Test
Repeated-Scan-Test
SPECIMEN
Ø=3mm
h=9.323 mm
VOI
lxpxh
180x180x932

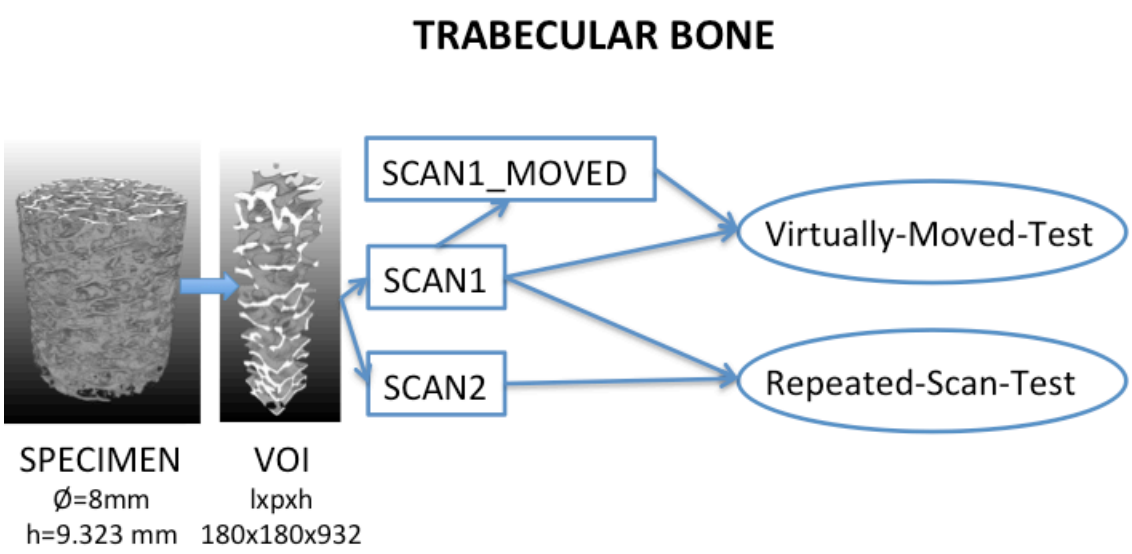
TRABECULAR BONE
SCAN1_MOVED
SCAN1
SCAN2
Virtually-Moved-Test
Repeated-Scan-Test
SPECIMEN
Ø=8mm
h=9.323 mm
VOI
lxpxh
180x180x932

Figure2

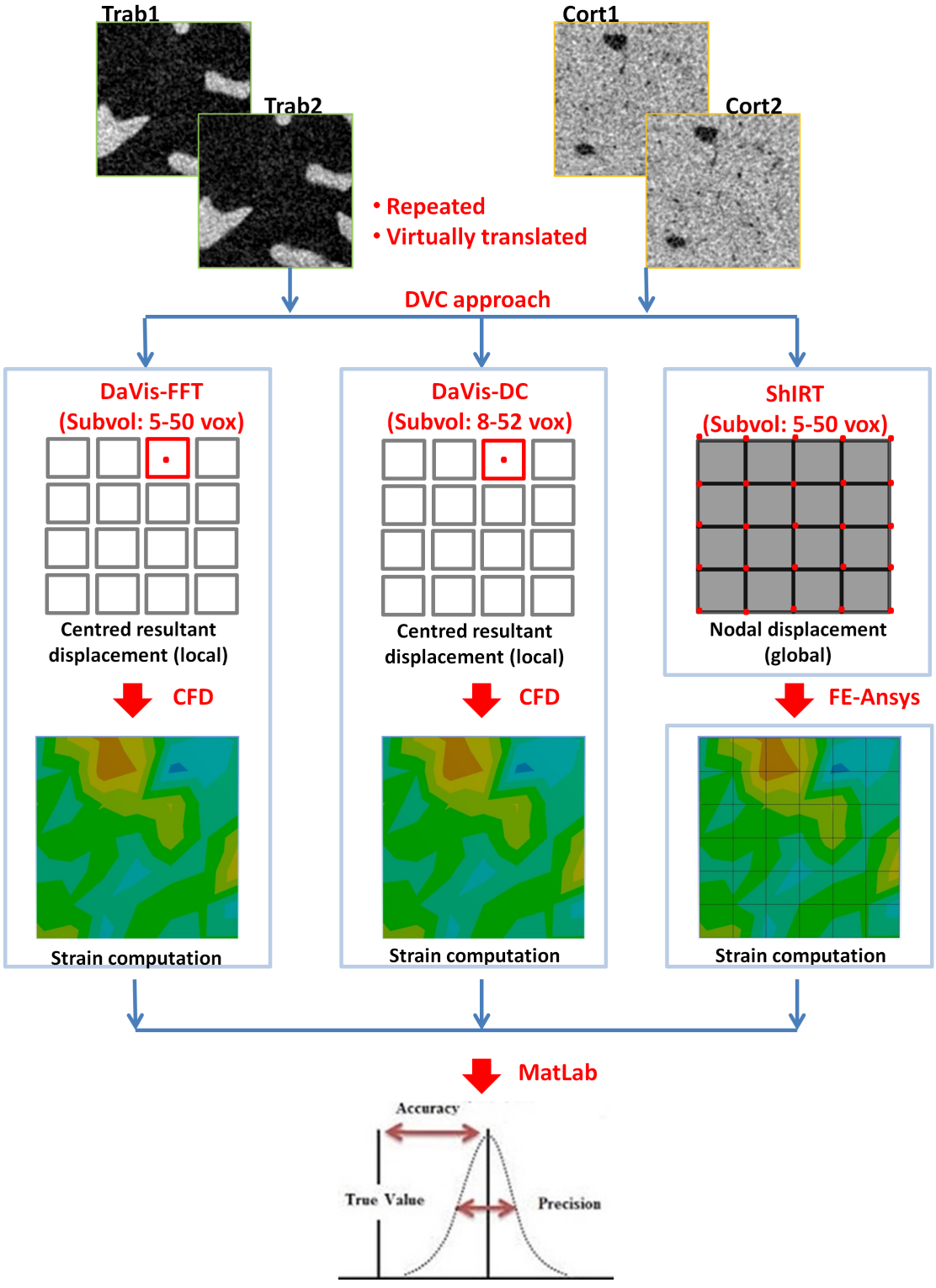
Trab1
Trab2
Cort1
Cort2
• Repeated
• Virtually translated
DVC approach
DaVis-FFT
(Subvol: 5-50 vox)
Centred resultant
displacement (local)
CFD
Strain computation
DaVis-DC
(Subvol: 8-52 vox)
Centred resultant
displacement (local)
CFD
Strain computation
ShIRT
(Subvol: 5-50 vox)
Nodal displacement
(global)
FE-Ansys
Strain computation
MatLab
Accuracy
True Value
Precision

Figure3

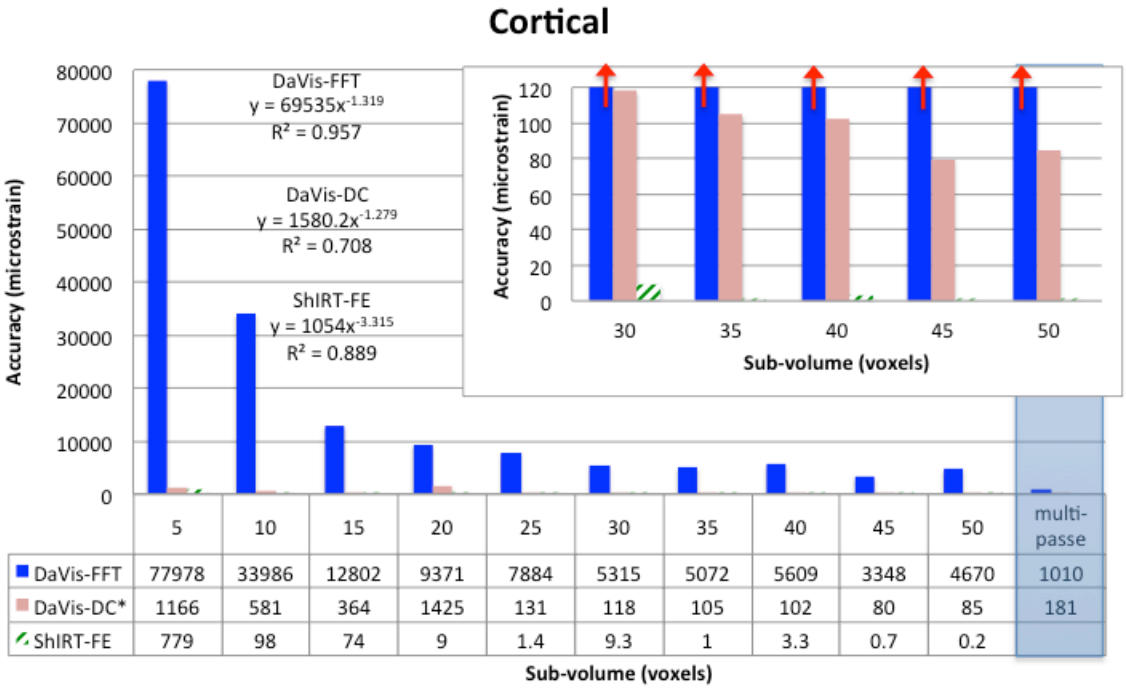
Cortical
Accuracy (microstrain)
DaVis-FFT
y = 69535x^-1.319
R² = 0.957
DaVis-DC
y = 1580.2x^-1.279
R² = 0.708
ShIRT-FE
y = 1054x^-3.315
R² = 0.889
Sub-volume (voxels)
5 10 15 20 25 30 35 40 45 50 multi-passe
DaVis-FFT 77978 33986 12802 9371 7884 5315 5072 5609 3348 4670 1010
DaVis-DC* 1166 581 364 1425 131 118 105 102 80 85 181
ShIRT-FE 779 98 74 9 1.4 9.3 1 3.3 0.7 0.2

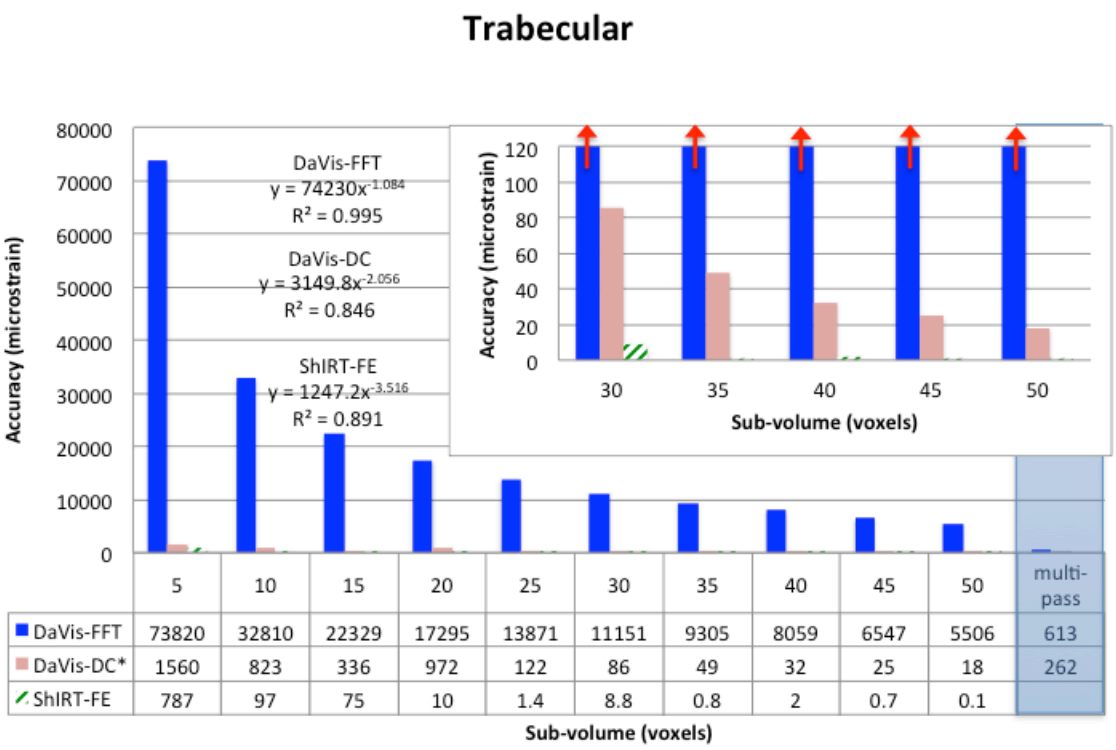
Trabecular
Accuracy (microstrain)
DaVis-FFT
y = 74230x^-1.084
R² = 0.995
DaVis-DC
y = 3149.8x^-2.056
R² = 0.846
ShIRT-FE
y = 1247.2x^-3.516
R² = 0.891
Sub-volume (voxels)
5 10 15 20 25 30 35 40 45 50 multi-pass
DaVis-FFT 73820 32810 22329 17295 13871 11151 9305 8059 6547 5506 613
DaVis-DC* 1560 823 336 972 122 86 49 32 25 18 262
ShIRT-FE 787 97 75 10 1.4 8.8 0.8 2 0.7 0.1

Figure4

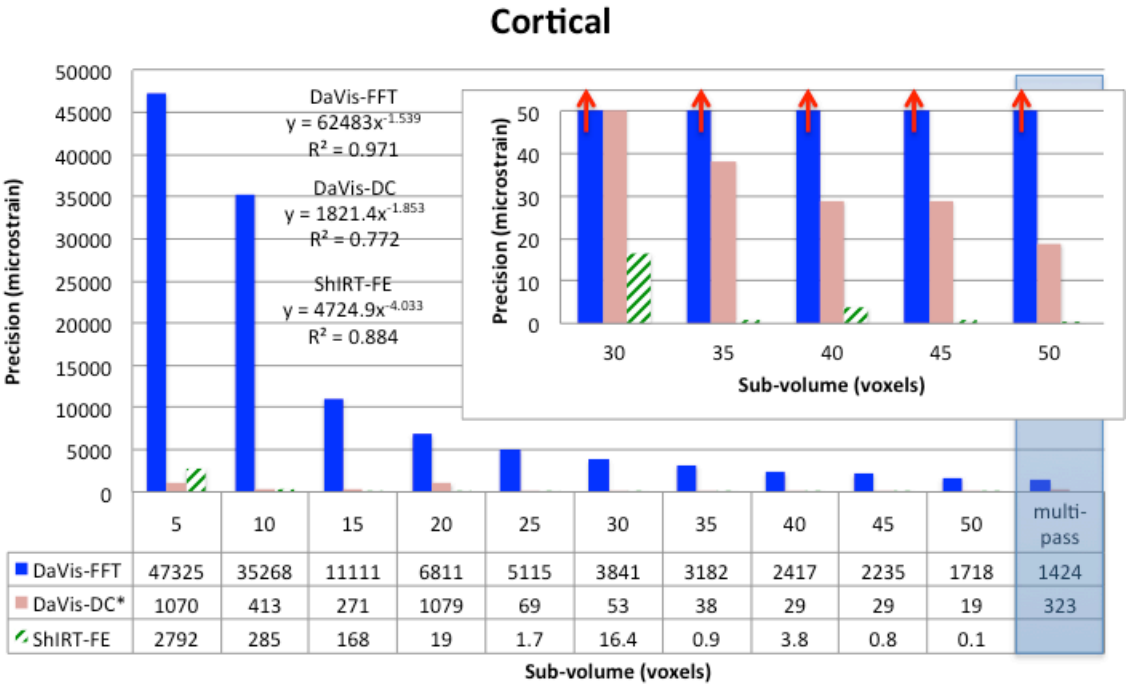

	5	10	15	20	25	30	35	40	45	50	multi-pass
DaVis-FFT	47325	35268	11111	6811	5115	3841	3182	2417	2235	1718	1424
DaVis-DC*	1070	413	271	1079	69	53	38	29	29	19	323
ShIRT-FE	2792	285	168	19	1.7	16.4	0.9	3.8	0.8	0.1	

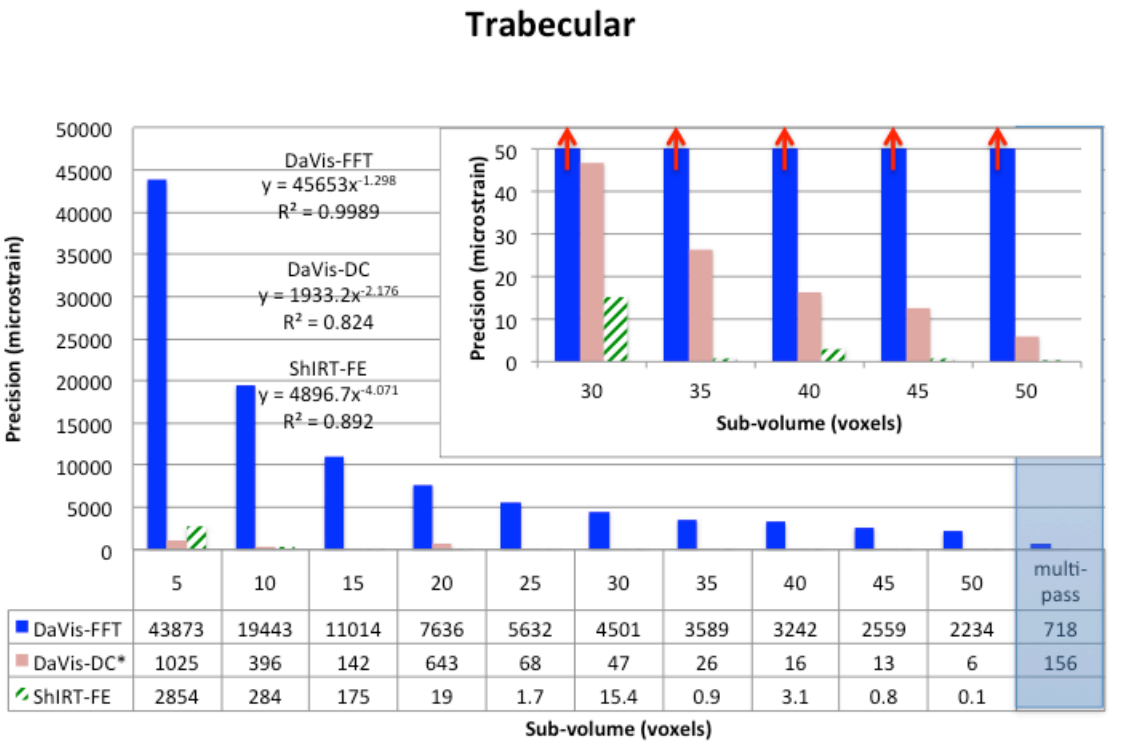

	5	10	15	20	25	30	35	40	45	50	multi-pass
DaVis-FFT	43873	19443	11014	7636	5632	4501	3589	3242	2559	2234	718
DaVis-DC*	1025	396	142	643	68	47	26	16	13	6	156
ShIRT-FE	2854	284	175	19	1.7	15.4	0.9	3.1	0.8	0.1	

Figure5

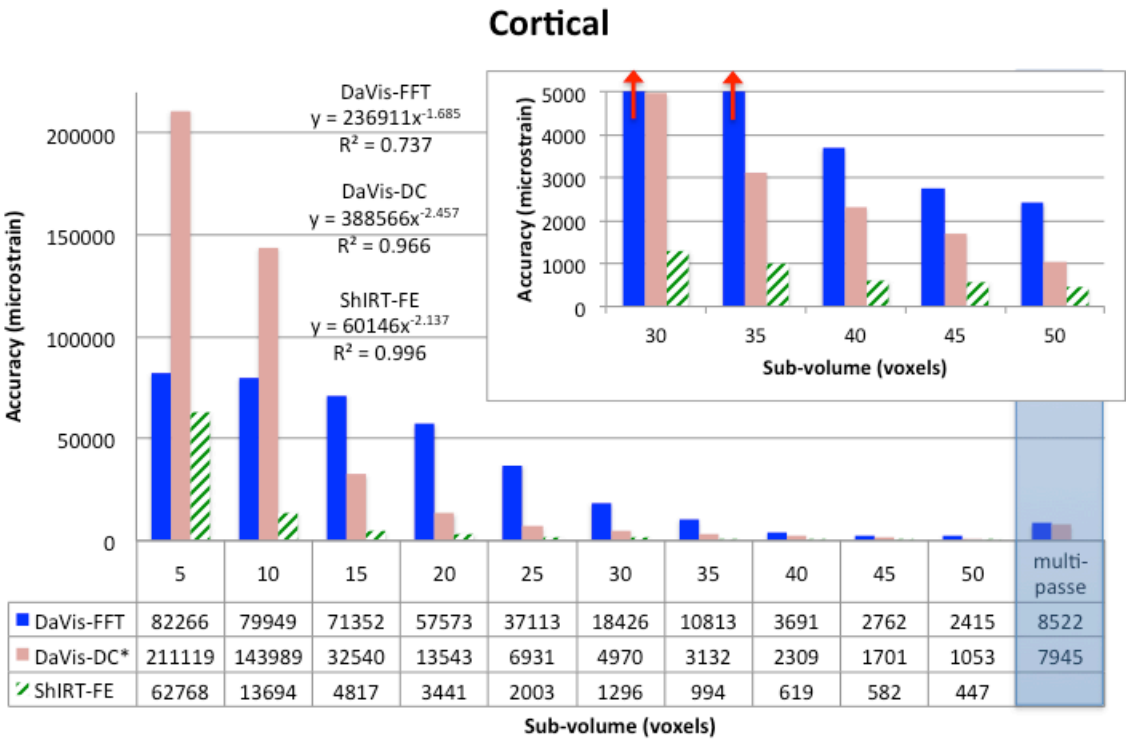
Cortical
DaVis-FFT
y = 236911x^-1.685
R² = 0.737
DaVis-DC
y = 388566x^-2.457
R² = 0.966
ShIRT-FE
y = 60146x^-2.137
R² = 0.996
Accuracy (microstrain)
Sub-volume (voxels)
5 10 15 20 25 30 35 40 45 50 multi-passe
DaVis-FFT 82266 79949 71352 57573 37113 18426 10813 3691 2762 2415 8522
DaVis-DC* 211119 143989 32540 13543 6931 4970 3132 2309 1701 1053 7945
ShIRT-FE 62768 13694 4817 3441 2003 1296 994 619 582 447

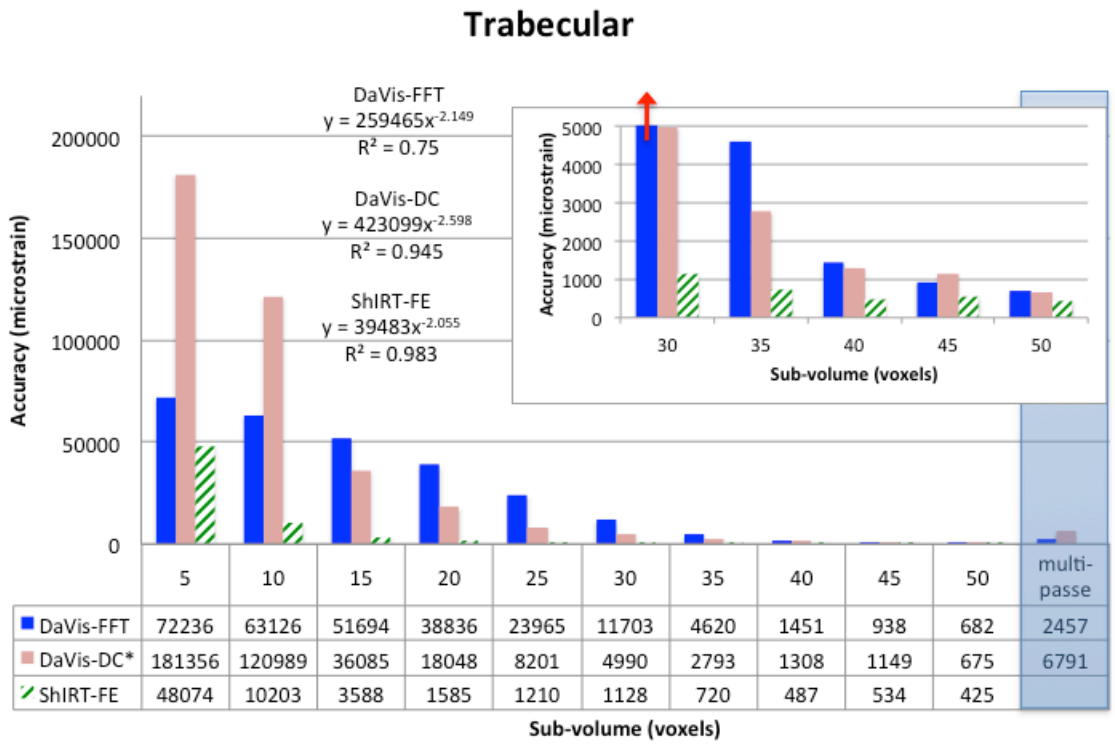
Trabecular
DaVis-FFT
y = 259465x^-2.149
R² = 0.75
DaVis-DC
y = 423099x^-2.598
R² = 0.945
ShIRT-FE
y = 39483x^-2.055
R² = 0.983
Accuracy (microstrain)
Sub-volume (voxels)
5 10 15 20 25 30 35 40 45 50 multi-passe
DaVis-FFT 72236 63126 51694 38836 23965 11703 4620 1451 938 682 2457
DaVis-DC* 181356 120989 36085 18048 8201 4990 2793 1308 1149 675 6791
ShIRT-FE 48074 10203 3588 1585 1210 1128 720 487 534 425

Figure6

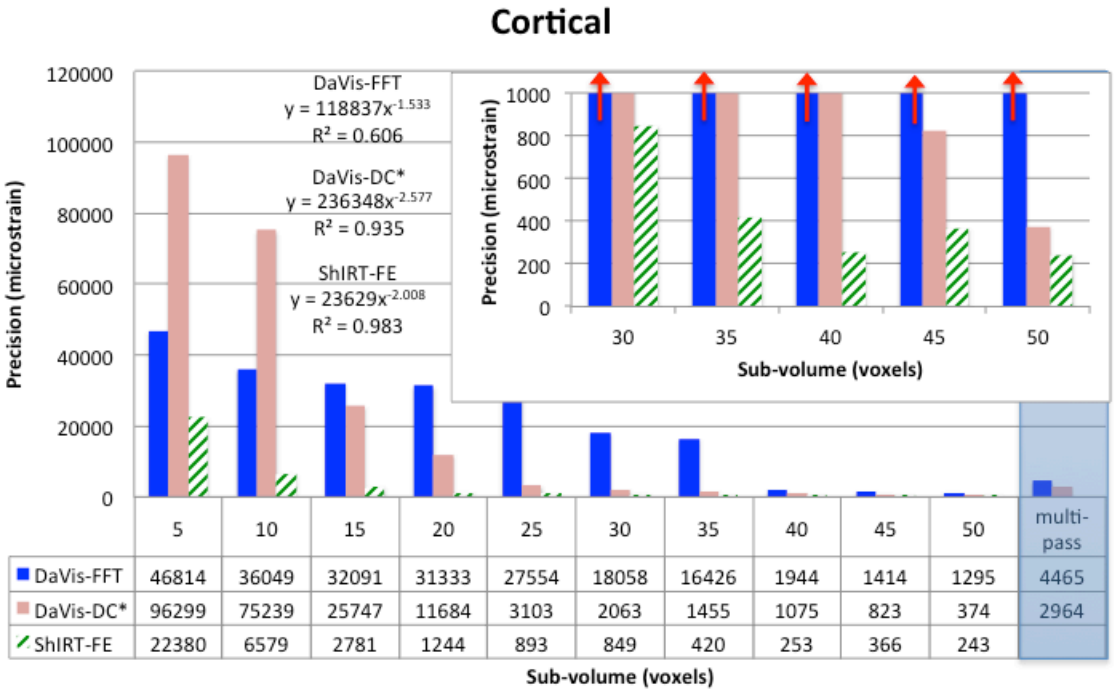

	5	10	15	20	25	30	35	40	45	50	multi-pass
DaVis-FFT	46814	36049	32091	31333	27554	18058	16426	1944	1414	1295	4465
DaVis-DC*	96299	75239	25747	11684	3103	2063	1455	1075	823	374	2964
ShIRT-FE	22380	6579	2781	1244	893	849	420	253	366	243	

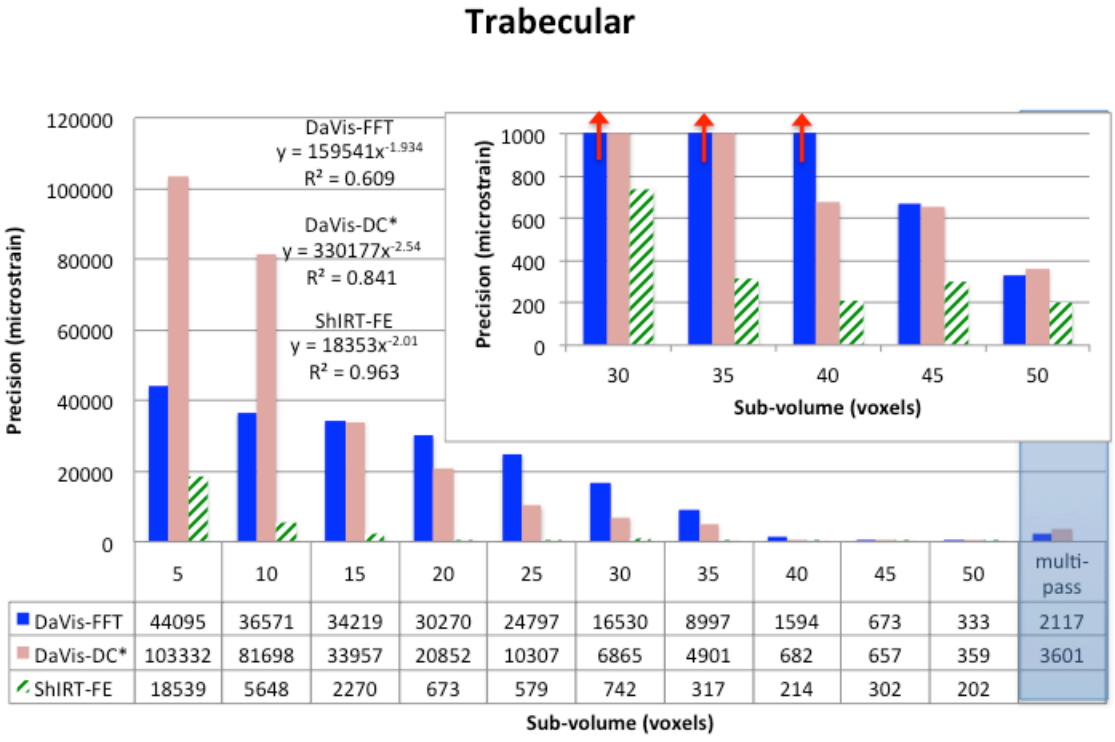

	5	10	15	20	25	30	35	40	45	50	multi-pass
DaVis-FFT	44095	36571	34219	30270	24797	16530	8997	1594	673	333	2117
DaVis-DC*	103332	81698	33957	20852	10307	6865	4901	682	657	359	3601
ShIRT-FE	18539	5648	2270	673	579	742	317	214	302	202	

Figure7

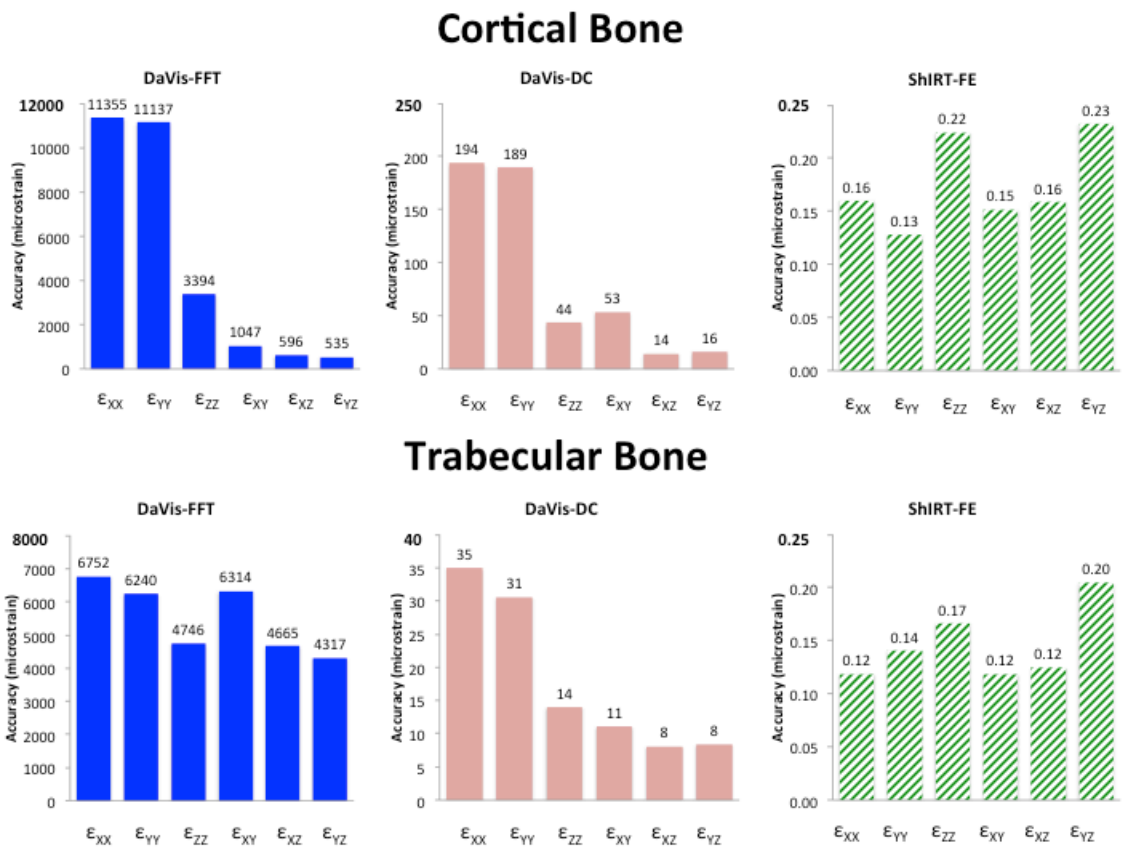
Cortical Bone
DaVis-FFT
DaVis-DC
ShIRT-FE
Accuracy (microstrain)
11355
11137
3394
1047
596
535
194
189
44
53
14
16
0.16
0.13
0.22
0.15
0.16
0.23
Trabecular Bone
6752
6240
4746
6314
4665
4317
35
31
14
11
8
8
0.12
0.14
0.17
0.12
0.12
0.20
εXX
εYY
εZZ
εXY
εXZ
εYZ

Figure8

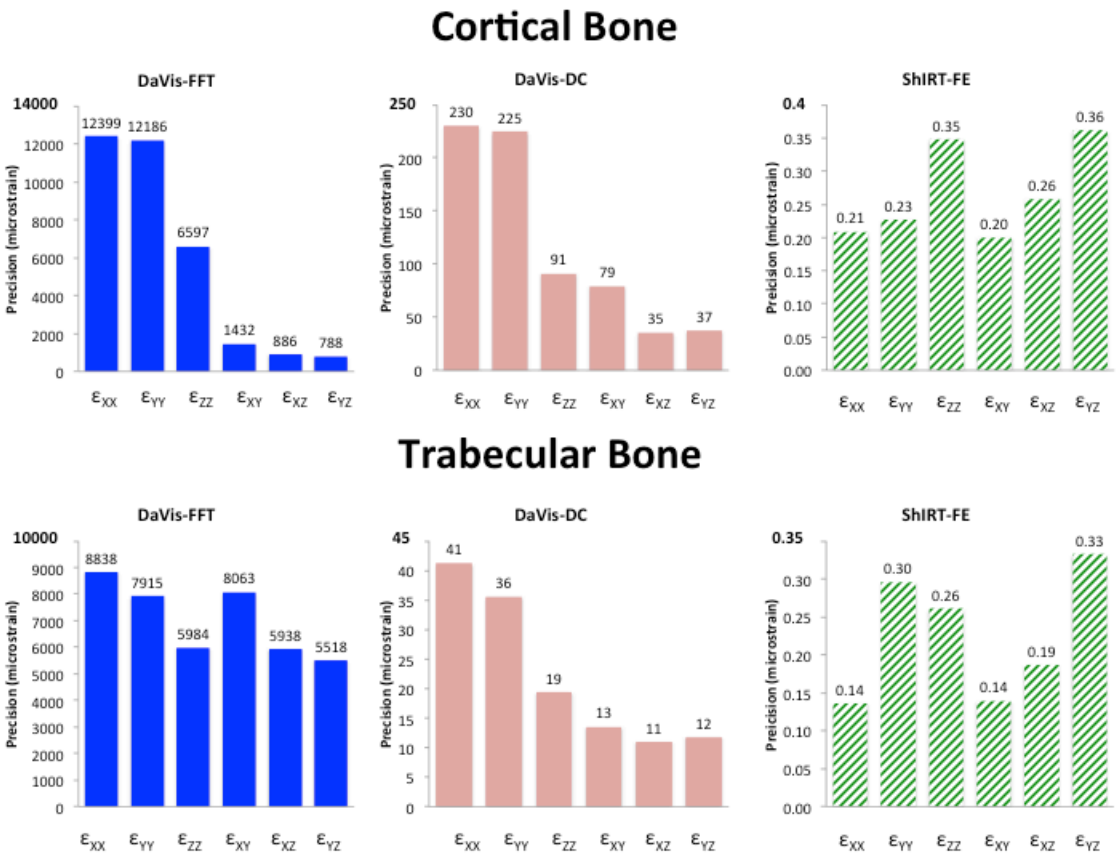
Cortical Bone
DaVis-FFT
Precision (microstrain)
14000
12000
10000
8000
6000
4000
2000
0
12399
12186
6597
1432
886
788
εXX εYY εZZ εXY εXZ εYZ
DaVis-DC
Precision (microstrain)
250
200
150
100
50
0
230
225
91
79
35
37
εXX εYY εZZ εXY εXZ εYZ
ShIRT-FE
Preicision (microstrain)
0.4
0.35
0.30
0.25
0.20
0.15
0.10
0.05
0.00
0.21
0.23
0.35
0.20
0.26
0.36
εXX εYY εZZ εXY εXZ εYZ
Trabecular Bone
DaVis-FFT
Precision (microstrain)
10000
9000
8000
7000
6000
5000
4000
3000
2000
1000
0
8838
7915
5984
8063
5938
5518
εXX εYY εZZ εXY εXZ εYZ
DaVis-DC
Precision (microstrain)
45
40
35
30
25
20
15
10
5
0
41
36
19
13
11
12
εXX εYY εZZ εXY εXZ εYZ
ShIRT-FE
Preicision (microstrain)
0.35
0.30
0.25
0.20
0.15
0.10
0.05
0.00
0.14
0.30
0.26
0.14
0.19
0.33
εXX εYY εZZ εXY εXZ εYZ

Figure9

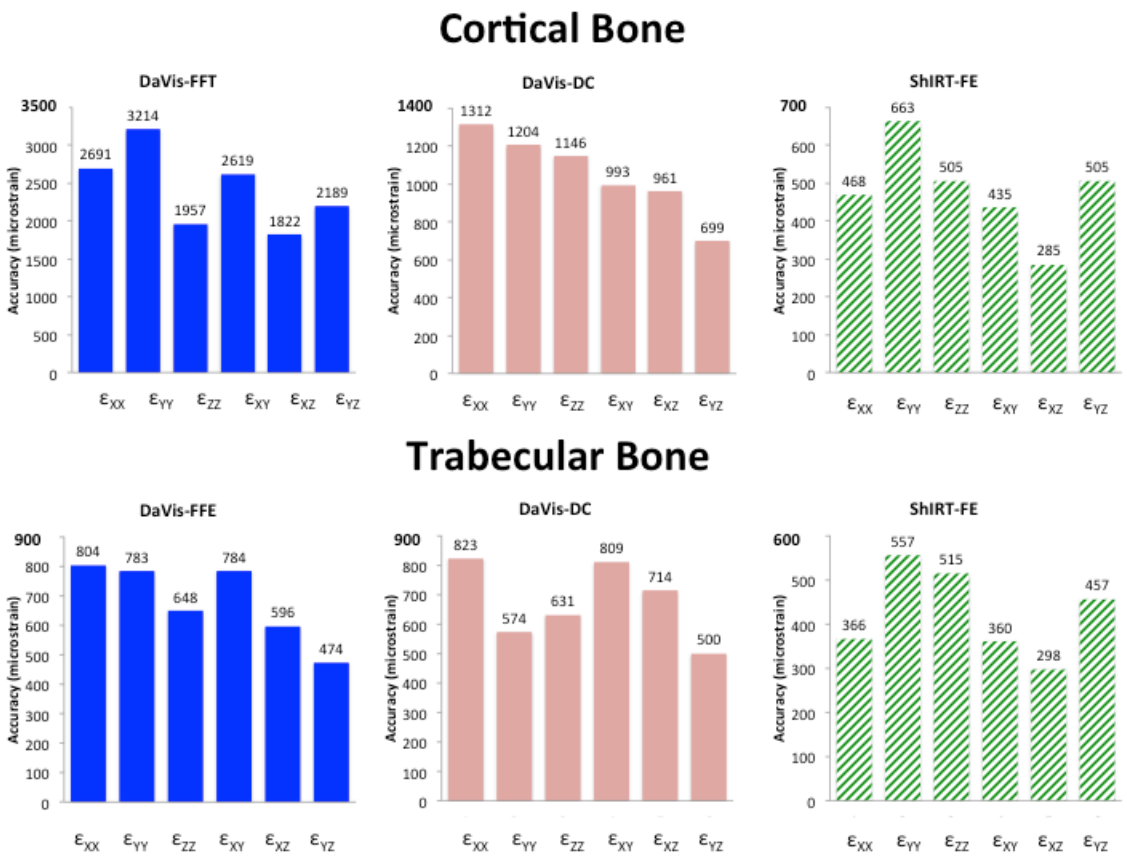
Cortical Bone
DaVis-FFT
Accuracy (microstrain)
3500
3000
2500
2000
1500
1000
500
0
2691
3214
1957
2619
1822
2189
εXX εYY εZZ εXY εXZ εYZ
DaVis-DC
1400
1200
1000
800
600
400
200
0
1312
1204
1146
993
961
699
ShIRT-FE
700
600
500
400
300
200
100
0
468
663
505
435
285
505
Trabecular Bone
DaVis-FFE
900
800
700
600
500
400
300
200
100
0
804
783
648
784
596
474
DaVis-DC
823
574
631
809
714
500
ShIRT-FE
600
500
400
300
200
100
0
366
557
515
360
298
457

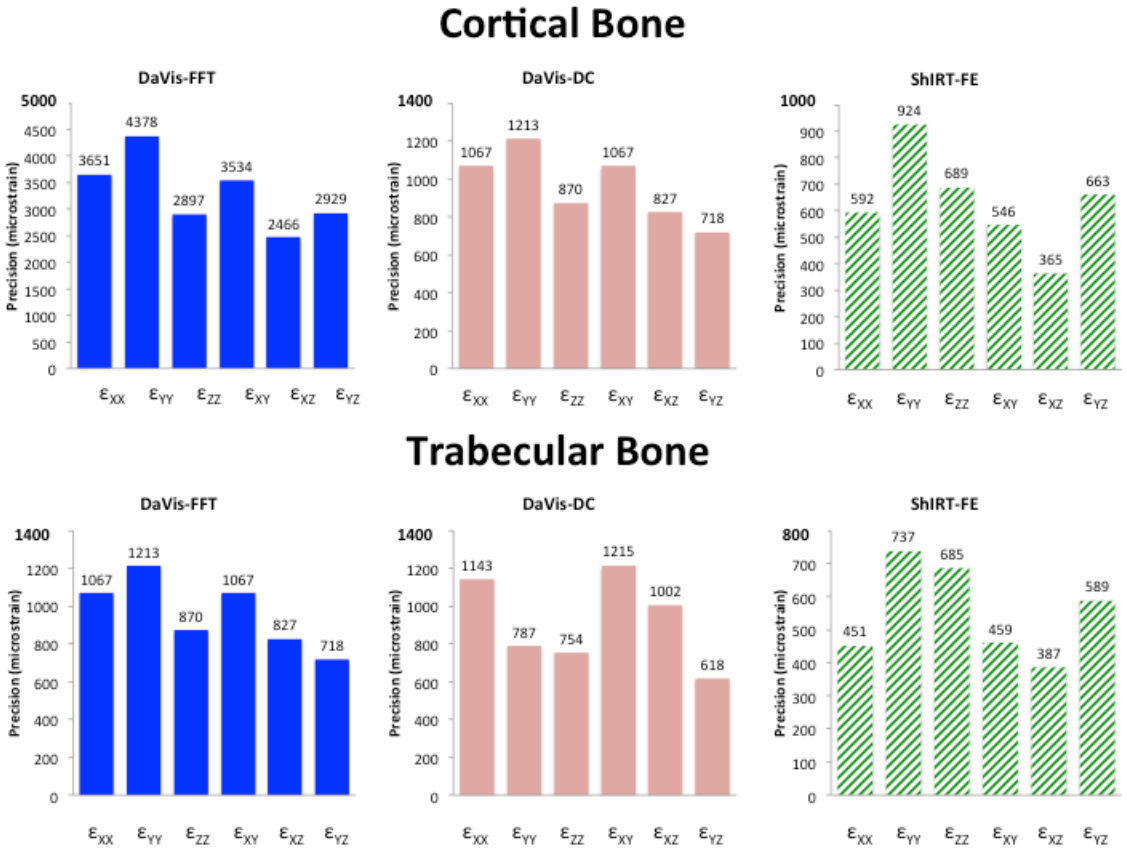
Cortical Bone
DaVis-FFT
Precision (microstrain)
5000
4500
4000
3500
3000
2500
2000
1500
1000
500
0
3651
4378
2897
3534
2466
2929
εXX εYY εZZ εXY εXZ εYZ
DaVis-DC
Precision (microstrain)
1400
1200
1000
800
600
400
200
0
1067
1213
870
1067
827
718
εXX εYY εZZ εXY εXZ εYZ
ShIRT-FE
Precision (microstrain)
1000
900
800
700
600
500
400
300
200
100
0
592
924
689
546
365
663
εXX εYY εZZ εXY εXZ εYZ
Trabecular Bone
DaVis-FFT
Precision (microstrain)
1400
1200
1000
800
600
400
200
0
1067
1213
870
1067
827
718
εXX εYY εZZ εXY εXZ εYZ
DaVis-DC
Precision (microstrain)
1400
1200
1000
800
600
400
200
0
1143
787
754
1215
1002
618
εXX εYY εZZ εXY εXZ εYZ
ShIRT-FE
Precision (microstrain)
800
700
600
500
400
300
200
100
0
451
737
685
459
387
589
εXX εYY εZZ εXY εXZ εYZ

BIBLIOGRAPHY

[1] Roberts, B. C., Perilli, E., and Reynolds, K. J., 2014, "Application of the digital volume correlation technique for the measurement of displacement and strain fields in bone: A literature review," Journal of biomechanics, 47(5), pp. 923-934.

[2] Bay, B. K., Smith, T. S., Fyhrie, D. P., and Saad, M., 1999, "Digital Volume Correaltion: Three-dimensional Strain Mapping Using X-ray Tomography," Experimental Mechanics, 39(3), pp. 217 - 226.

[3] Gates, M., Lambros, J., and Heath, M. T., 2010, "Towards High Performance Digital Volume Correlation," Experimental Mechanics, 51(4), pp. 491-507.

[4] Barber, D. C., Oubel, E., Frangi, A. F., and Hose, D. R., 2007, "Efficient computational fluid dynamics mesh generation by image registration," Med Image Anal, 11(6), pp. 648-662.

[5] Khodabakhshi, G., Walker, D., Scutt, A., Way, L., Cowie, R. M., and Hose, D. R., 2013, "Measuring three-dimensional strain distribution in tendon," J Microsc, 249(3), pp. 195-205.

[6] Gillard, F., Boardman, R., Mavrogordato, M., Hollis, D., Sinclair, I., Pierron, F., and Browne, M., 2014, "The application of digital volume correlation (DVC) to study the microstructural behaviour of trabecular bone during compression," J Mech Behav Biomed Mater, 29, pp. 480-499.

[7] Madi, K., Tozzi, G., Zhang, Q. H., Tong, J., Cossey, A., Au, A., Hollis, D., and Hild, F., 2013, "Computation of full-field displacements in a scaffold implant using digital volume correlation and finite element analysis," Med Eng Phys, 35(9), pp. 1298-1312.

[8] Liu, L., and Morgan, E. F., 2007, "Accuracy and precision of digital volume correlation in quantifying displacements and strains in trabecular bone," Journal of biomechanics, 40(15), pp. 3516-3520.

[9] Dall'Ara, E., Barber, D., and Viceconti, M., 2014, "About the inevitable compromise between spatial resolution and accuracy of strain measurement for bone tissue: A 3D zero-strain study," Journal of biomechanics, 47(12), pp. 2956-63

[10] Tozzi, G., Zhang, Q. H., and Tong, J., 2014, "Microdamage assessment of bone-cement interfaces under monotonic and cyclic compression," Journal of biomechanics, 47(14), pp. 3466-74

[11] Pan, B., Wang, B., Wu, D., and Lubineau, G., 2014, "An efficient and accurate 3D displacements tracking strategy for digital volume correlation," Optics and Lasers in Engineering, 58, pp. 126-135.

[12] Christen, D., Levchuk, A., Schori, S., Schneider, P., Boyd, S. K., and Muller, R., 2012, "Deformable image registration and 3D strain mapping for the quantitative assessment of cortical bone microdamage," Journal of Mechanical Behavior of Biomedical Materials, 8, pp. 184-193.

[13] Smith, T. S., Bay, B. K., and Rashid, F., 2002, "Digital Volume Correlation Inclunding Rotational Degrees of Freedom during Minimization," Experimental Mechanics, 42(3), pp. 272 - 278.

[14] Roux, S., Hild, F., Viot, P., and Bernard, D., 2008, "Three-dimensional image correlation from X-ray computed tomography of solid foam," Composites Part A: Applied Science and Manufacturing, 39(8), pp. 1253-1265.

[15] Benoit, A., Guerard, S., Gillet, B., Guillot, G., Hild, F., Mitton, D., Perie, J. N., and Roux, S., 2009, "3D analysis from micro-MRI during in situ compression on cancellous bone," Journal of biomechanics, 42(14), pp. 2381-2386.

[16] Hussein, A. I., Barbone, P. E., and Morgan, E. F., 2012, "Digital Volume Correlation for Study of the Mechanics of Whole Bones," Procedia IUTAM, 4, pp. 116-125.

[17] Hussein, A. I., Mason, Z. D., and Morgan, E. F., 2013, "Presence of intervertebral discs alters observed stiffness and failure mechanisms in the vertebra," Journal of biomechanics, 46(10), pp. 1683-1688.

[18] Cheminet, A., Leclaire, B., Champagnat, F., Plyer, A., Yegavian, R., and Le Besnerais, G., 2014, "Accuracy assessment of a Lucas-Kanade based correlation method for 3D PIV," 17th Internation Symposium on Applications of Laser Techniques to Fluid Mechanics, Lisbon, Portugal, 07-10 July.

[19] Scarano, F., 2013, "Tomographic PIV: principles and practice," Measurement Science and Technology, 24(1), p. 012001.

[20] Barber, D. C., and Hose, D. R., 2005, "Automatic segmentation of medical images using image registration: diagnostic and simulation applications," J Med Eng&Tech, 29(2), pp. 53-63.

[21] Hild, F., and Roux, S., 2012, "Comparison of local and global approaches to digital image correlation," Experimental Mechanics, 52(9), pp. 1503-1519.

[22] Nicolella, D. P., Nicholls, A. E., Lankford, J., and Davy, D. T., 2001, "Machine vision photogrammetry: a technique for measurement of microstructural strain in cortical bone," Journal of biomechanics, 34(1), pp. 135-9.

[23] Lionello, G., and Cristofolini, L., 2014, "A practical approach to optimizing the preparation of speckle patterns for digital-image correlation," Measurement Science and Technology, 25(10), p. 107001.

[24] Fung, Y. C., 1980, "Bone and cartilage," Biomechanics - Mechanical properties of living tissues, Springer Verlag, New York, pp. 383-415.

[25] Currey, J. D., 1982, "Bone as a mechanical structure," Biomechanics - Principles and applications, 1, pp. 75-85.

[26] Bayraktar, H. H., Morgan, E. F., Niebur, G. L., Morris, G. E., Wong, E. K., and Keaveny, T. M., 2004, "Comparison of the elastic and yield properties of human femoral trabecular and cortical bone tissue," Journal of biomechanics, 37(1), pp. 27-35.

[27] Ohman, C., Dall'Ara, E., Baleani, M., Van Sint Jan, S., and Viceconti, M., 2008, "The effects of embalming using a 4% formalin solution on the compressive mechanical properties of human cortical bone," Clinical biomechanics, 23(10), pp. 1294-1298.